

# High-pressure x-ray diffraction studies on the structure of liquid silicate using a Paris–Edinburgh type large volume press

Akihiro Yamada,<sup>1,a)</sup> Yanbin Wang,<sup>2</sup> Toru Inoue,<sup>1</sup> Wenge Yang,<sup>3,b)</sup> Changyong Park,<sup>3</sup> Tony Yu,<sup>2</sup> and Guoyin Shen<sup>3</sup>

<sup>1</sup>*Geodynamics Research Center, Ehime University, 2-5 Bunkyo-cho, Matsuyama 790-0855, Japan*

<sup>2</sup>*Center for Advanced Radiation Sources, The University of Chicago, 5640 S. Ellis Ave., Chicago, Illinois 60637, USA*

<sup>3</sup>*HPCAT, Carnegie Institute of Washington, Argonne, Illinois 60439-4803, USA*

(Received 4 August 2010; accepted 12 October 2010; published online 10 January 2011)

An experimental setup for high-pressure liquid structure studies with synchrotron x-ray diffraction using the Paris–Edinburgh press has been installed at station 16-BM-B (HPCAT) of the Advanced Photon Source, Argonne National Laboratory. By collecting energy-dispersive data with a synchrotron white beam at various  $2\theta$  angles, the present device allows us to obtain the structure factor,  $S(Q)$ , over a wide range of  $Q$  ( $= 4\pi \sin\theta/\lambda$ ) owing to the excellent angular accessibility up to  $37^\circ$  in  $2\theta$  and high energy photons well beyond 100 keV. We have successfully collected XRD data on silicate (albite,  $\text{NaAlSi}_3\text{O}_8$ ) liquids with  $Q$  up to  $\sim 22 \text{ \AA}^{-1}$  and pressure up to 5.3 GPa and temperature 1873 K, and obtained the radial distribution function,  $G(r)$ , with a reasonable resolution. The T–O bond length (where T = Al, Si), which is a fundamental measure of local structure for aluminous silicate consisting of  $\text{SiO}_n$  and  $\text{AlO}_n$  polyhedra (tetrahedra at 1 atm condition), was found to be slightly shortened to 1.626 Å compared to that of glass at 1 atm. The T–O–T bond angle, which is the linkage of the above polyhedra, is the most responsible for densification. The T–O–T peak in  $G(r)$  splits into two peaks, suggesting a differentiation of the bond angle at high-pressure. The present technical development demonstrates that the Paris–Edinburgh press is suitable for studies of silicate liquids under high-pressure conditions. © 2011 American Institute of Physics. [doi:10.1063/1.3514087]

## I. INTRODUCTION

*In situ* studies on the structure of molten silicates are still challenging due to their refractory nature (which requires higher temperature generation) and low scattering power (which requires larger sample volume). So far, high-pressure x-ray diffraction (XRD) for liquid silicates has been performed on multianvil apparatus such as the Kawai-type and DIA-type large volume presses (LVP) with polychromatic x-rays (e.g., DIA type;<sup>1</sup> Kawai type<sup>2</sup>). In previous studies, using the DIA-type multianvil apparatus, the  $2\theta$  angle was limited to below  $25^\circ$  (e.g., Refs. 1 and 3) due to the geometrical constraints of the LVP. In these studies, the maximum momentum transfer,  $Q$ , has been limited to  $\sim 15 \text{ \AA}^{-1}$ . In order to obtain more believable results from the radial distribution function, which is derived by a Fourier transformation of the structure factor, higher- $Q$  data are strongly required. Thus, it is necessary to develop apparatus with higher diffraction angle ( $2\theta$ ) accessibility. In this report, we demonstrate the application of the Paris–Edinburgh press (PEP) (e.g., Ref. 4) for high-pressure XRD on silicate liquids, to investigate local structural change with pressure. The present apparatus has a wide-angle accessibility in the horizontal plane and a relatively large sample volume. Previous studies have shown that the apparatus is capable of gener-

ating stable high temperatures at modest pressures [e.g., 2473 K and 0.3 GPa (Ref. 5), 1000 K and  $<15$  GPa (Ref. 6)]. However, the PEP has not been applied to investigate structures of liquid silicates.

In this paper, we present new developments for studying the structures of silicate liquids and glasses with the Paris–Edinburgh press. In addition, we demonstrate a successful application of high-pressure and temperature experiments on the structure of aluminous silicate liquid,  $\text{NaAlSi}_3\text{O}_8$ . The present technical development broadens the application of the device for studying the structure and physicochemical properties of silicate liquids at high-pressure.

## II. EXPERIMENTAL SETUP

### A. Setup for high-pressure x-ray diffraction

High-pressure multiangle energy-dispersive x-ray diffraction (EDXD) for liquid silicates has been performed at the Sector 16-BM-B beamline, High Pressure Collaborative Access Team (HPCAT) at the Advanced Photon Source, Argonne National Laboratory. A portable system developed at GSECARS, the University of Chicago, was used for pressure and temperature generation. This system consists of a 230-ton Paris–Edinburgh press (e.g., Ref. 4) with a double-stage pressure controller. In our experiment, newly designed anvils (tungsten carbide alloy; VF12, Fuji Dies Co., Ltd.) with a flattened bottom were adapted (Fig. 1). Polychromatic x-rays with a wide range of energy (up to  $\sim 150$  keV) from the bending magnet source are available at the beamline.

<sup>a)</sup> Author to whom correspondence should be addressed. Electronic mail: a-yamada@sci.ehime-u.ac.jp. Tel.: +81-89-927-8151. FAX: +81-89-927-8167.

<sup>b)</sup> Present address: HPSynC, Carnegie Institution of Washington, Argonne, Illinois 60439-4803, USA.

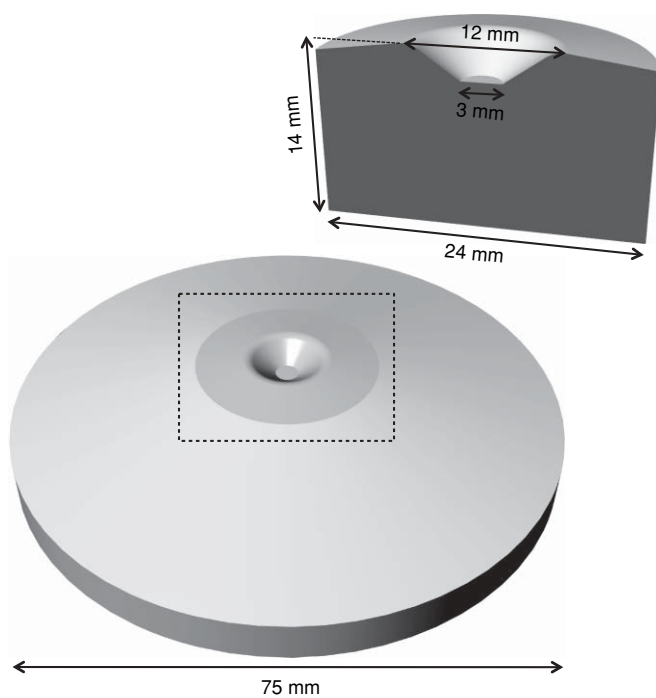


FIG. 1. Illustration of the newly designed anvil. Surrounded area with dashed line is the tungsten carbide alloy surrounded with steel base. Upper illustration is the cross-sectional part of the tungsten carbide.

A large Huber stage holding the energy-dispersive Ge solid-state detector (SSD) with high precision in mechanical  $2\theta$  was installed at the beamline. The maximum  $2\theta$  angle is about  $37^\circ$ . Incident x-rays were collimated by two pairs of slits made of tungsten to  $0.3 \text{ mm} \times 0.1 \text{ mm}$  (vertical  $\times$  horizontal). Diffracted x-rays were collimated horizontally to  $0.1 \text{ mm}$  by a pair of collimator slits and finally to  $0.5 \text{ mm} \times 0.2 \text{ mm}$  (vertical  $\times$  horizontal) by another pair of slits located immediately in front of the SSD. Diffraction patterns of the liquid sample were collected at  $\sim 10$   $2\theta$  angles between  $3^\circ$  and  $37^\circ$ , to cover a wide range of  $Q$  ( $= 4\pi E \sin \theta / 12.398$ , where  $E$  is the energy of the x-rays in keV). In collecting the diffraction signals from the liquid sample, the size of the slits was adjusted according to the  $2\theta$  angles so that the diffraction volume was kept approximately constant and the dead time of the SSD did not exceed 20%.

## B. Starting material and pressure–temperature generation

The starting material, an  $\text{NaAlSi}_3\text{O}_8$  glass, was prepared by melting a powdered oxide mixture of  $\text{Na}_2\text{CO}_3$ ,  $\text{Al}_2\text{O}_3$ , and  $\text{SiO}_2$  (molar ratio 1:1:6) at 1573 K and quenching in air to room temperature. Before melting, the sample was held at 1273 K for 9 h to degas  $\text{CO}_2$  from  $\text{NaCO}_3$ . The quenched sample was colorless, although small bubbles were present. X-ray diffraction on the sample confirmed that it was in a glass phase, with no sharp diffraction peaks. The obtained chunk of glass was then ground to powder for the high-pressure and temperature experiments.

The high-pressure and temperature cell assembly used in this study is shown in Fig. 2. The main features of the

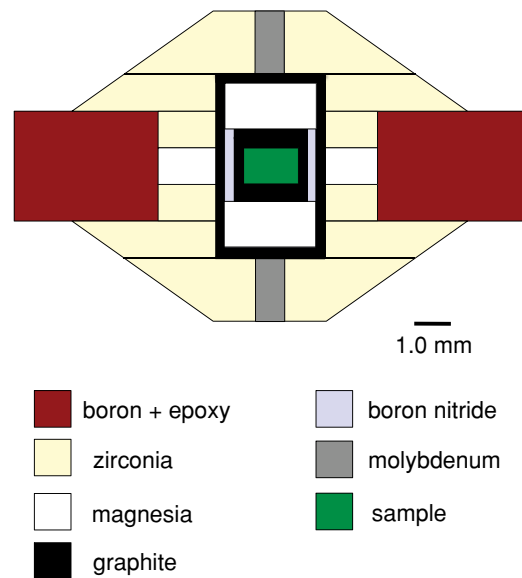


FIG. 2. (Color online) A cross section of the cell assembly used in the experiment on liquid silicate.

assembly are (1) large sample volume, (2) high thermal insulation, and (3) high transparency of x-rays. The initial dimensions of the sample were 1.5 mm in diameter and 1.25 mm in height. In order to minimize heat loss at high temperatures, semi-sintered zirconia (OZ-8C; Mino Ceramic Co., Ltd.) was used as a thermal insulator all around the graphite heater except for the x-ray path. Semi-sintered magnesia (OM; Mino Ceramic Co., Ltd.) was placed in the path of the x-rays and was also used for pressure measurement (equation of state for  $\text{MgO}$  used<sup>7</sup>). A ring made of boron epoxy (BE; 4:1 with weight ratio) was used as a gasket, which was isolated from the graphite heater by zirconia and magnesia rings, because epoxy in the BE component degasses at temperatures greater than  $\sim 700 \text{ K}$ . The BE gasket is also a good thermal insulator and mechanically strong, which helped maintain a wide vertical anvil gap, so that more diffraction signals could be collected from the liquid sample. Temperature was estimated based on the melting curve of  $\text{NaAlSi}_3\text{O}_8$  (e.g., Ref. 8). Also, the relationship between power consumption and temperature from a separate experiment using a W3%Re–W25%Re thermocouple was used to guide the temperature estimation. Estimated uncertainty in temperature was within 10%. Melting of the sample was easily recognized. The glass sample crystallized at around 900 K (depends on pressure), exhibiting many crystalline peaks. With further increase in temperature, all crystalline peaks disappeared indicating melting.

## C. Analytical method for liquid/amorphous structure

We used the energy-dispersive x-ray diffraction technique, with data collected at multiple  $2\theta$  angles, for structural analysis. This method is useful for light scatters, especially for measurements conducted within high-pressure devices, which has a relatively simple diffraction geometry and high collimation capability. However, the analysis procedure is

more complicated than in the case of the angle-dispersive diffraction method, because the diffraction data are collected independently at several  $2\theta$  angles, and one needs to determine a common normalization factor in order to combine all the data collected at various  $2\theta$  angles. The basic procedure of the analysis for the data obtained by EDXD was first established by Ref. 9. Based on this idea, a new software package<sup>10</sup> has been developed for structural analyses of amorphous and liquid materials using polychromatic x-rays. With this software, one can obtain a unique intensity profile with energy to normalize the diffraction data collected at all  $2\theta$  angles. Obtaining a reliable intensity profile is the key for structural determination using the EDXD technique.<sup>11</sup> In general, the scattering intensity  $I_{\text{obs}}(E, \theta)$ , from a sample through a cell assembly, can be simply expressed as the following:

$$I_{\text{obs}}(E, \theta) = kI_{\text{eff}}(E)\{I_{\text{coh}}(E, \theta) + I_{\text{inc}}(E, \theta)\} + A_{\text{coh}}(E, \theta)I_{\text{back}}(E, \theta), \quad (1)$$

where  $k$ ,  $I_{\text{coh}}(E, \theta)$ ,  $I_{\text{inc}}(E, \theta)$ ,  $A_{\text{coh}}(E, \theta)$ , and  $I_{\text{back}}(E, \theta)$  are the normalization factor, coherent scattering intensity, incoherent scattering intensity, absorption factor, and intensity of back ground, respectively. The term  $A_{\text{coh}}(E, \theta)$  and  $I_{\text{back}}(E, \theta)$  can be estimated from the measurement of a dummy cell assembly without a sample. In our analysis, normalized x-ray scattering intensity of the sample,  $I(Q)$ , can be obtained successfully without correcting  $I_{\text{back}}(E, \theta)$  and  $A_{\text{coh}}(E, \theta)$ , indicating that the XRD data set has been collected with high signal-to-noise ratio. *Effective source intensity*,<sup>10</sup>  $I_{\text{eff}}(E)$ , can be uniquely determined by the software developed by Ref. 10.  $I_{\text{eff}}(E)$  is defined by the following relation:

$$I_{\text{eff}}(E) = I_p(E)C(E)A(E, \theta), \quad (2)$$

where  $I_p(E)$ ,  $C(E)$ , and  $A(E, \theta)$  are initial x-ray source intensity profile, detection efficiency of the SSD, and absorption, respectively. The absorption of the sample itself and materials of the cell assembly are included in  $I_{\text{eff}}(E)$ .

This method has been used successfully in many studies on amorphous and liquid structures from light to heavy materials at high-pressure with polychromatic x-rays (e.g., liquid hydrous Mg silicate;<sup>1</sup> liquid phosphorous;<sup>12</sup> liquid tin iodide<sup>13</sup>). Multiple data sets collected at various  $2\theta$  angles and normalization factors  $k$  [each one is described as Eq. (1)] are combined to construct the scattering intensity curve using the  $I_{\text{eff}}(E)$  shown as Eq. (2). The scattering intensity curve is then normalized to the  $I(Q)$  using atomic scattering factor,  $f(Q)$ , as shown in Fig. 3. Atomic scattering factor of an atom,  $f(Q)$ , is expressed as follows:

$$f(Q) = \sum_{j=1}^4 a_j \exp(-b_j s^2) + c, \quad (3)$$

where  $a_j$ ,  $b_j$ , and  $c$  are atomic-dependent parameters listed in Ref. 14. The variable  $s$  in this equation is given by  $Q/4\pi$ . To derive the coherent scattering intensity,  $I_{\text{coh}}(Q)$ , the component of incoherent scattering intensity,  $I_{\text{inc}}(Q)$ , is subtracted from the  $I(Q)$  (Fig. 3). The incoherent scattering intensity as

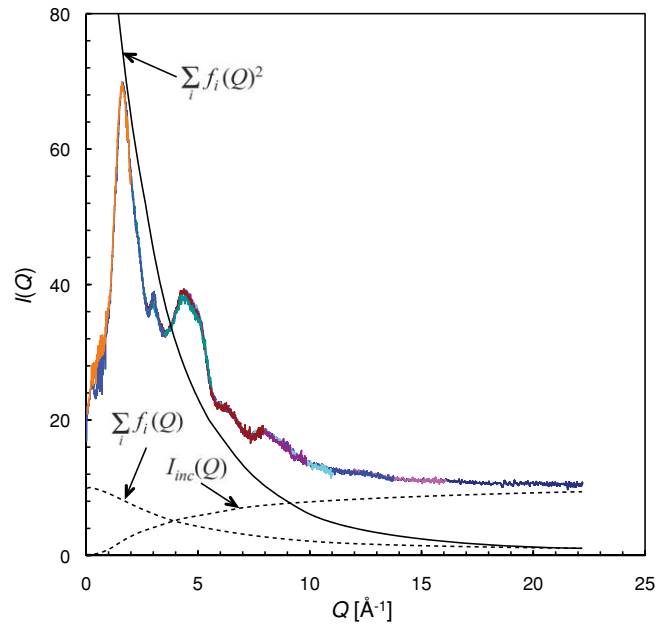


FIG. 3. (Color online) Normalized scattering intensity,  $I(Q)$ , of  $\text{NaAlSi}_3\text{O}_8$  glass at 1 atm plotted with average atomic scattering intensities [Eq. (3), solid and dotted line] and incoherent scattering intensity,  $I_{\text{inc}}(Q)$  [Eq. (4), dashed line]. Patterns overlapping  $I(Q)$  show the difference in data interval of each  $2\theta$  from  $3^\circ$  to  $37^\circ$ .

a function of  $Q$  can be derived based on a model calculation proposed by Refs. 15 and 16, and is expressed with Eq. (3),  $f(Q)$ , as the following:

$$I_{\text{inc}}(Q)s = Z - \left[ \frac{f(Q)^2 s}{2} \right] \times [1 - M(\exp\{-Ks\} - \exp\{Ls\})], \quad (4)$$

where  $M$ ,  $K$ , and  $L$  are the individual parameters for each atoms determined by Ref. 17.  $Z$  is the atomic number. The structure factor,  $S(Q)$ , is described with  $I_{\text{coh}}(Q)$  and the average atomic scattering intensity,  $\Sigma f_i(Q)$ , which can be calculated with Eq. (3), as the following relationship:

$$S(Q) = \frac{I_{\text{coh}}(Q) - \sum_i f_i(Q)^2}{\{\sum_i f_i(Q)\}^2} + 1. \quad (5)$$

The specific configuration of the average atomic scattering intensities for  $\text{NaAlSi}_3\text{O}_8$  composition are plotted in Fig. 3. Then, to obtain local structural information from  $S(Q)$ , the reduced radial distribution function,  $G(r)$ , which is the Fourier transformation of Eq. (5) and established by Ref. 18, is exploited. It can be derived without density information as follows:

$$G(r) = \frac{2}{\pi} \sum_m K_m^2 \int_0^\infty \{S(Q) - 1\} Q \sin(Qr) dQ, \quad (6)$$

where  $K$  is effective number of electrons for each atom, and approximately equals to the total number of electrons. For the purpose of comparison with previous results, the radial

distribution function,  $D(r)$ , which is also the Fourier transformation of Eq. (5), was also calculated for the analysis of the glass sample at 1 atm condition.  $D(r)$  in this study was derived using the density ( $2.369 \text{ g/cm}^3$ ) reported by a previous study:<sup>19</sup>

$$D(r) = 4\pi r^2 \rho_0 + \frac{2\pi}{r} \int_0^\infty \{S(Q) - 1\} Q \sin(Qr) dQ, \quad (7)$$

where  $r$  and  $\rho_0$  are radial distance in real spacing and average number of density, respectively. When the density of a liquid/amorphous material is known,  $D(r)$ , Eq. (7) is useful for more quantitative information about the structure (i.e., coordination number for each atom). However,  $G(r)$  alone as described by Eq. (6) is a useful tool for extracting information about the local structure, as the density of liquid/amorphous material at high-pressure and temperature is often not well known.

### III. EXPERIMENTAL RESULTS

#### A. Structure of NaAlSi<sub>3</sub>O<sub>8</sub> glass at ambient condition

We first collected data on the NaAlSi<sub>3</sub>O<sub>8</sub> glass loaded in the cell in Fig. 2 at 1 atm and room temperature [Fig. 4(a)] and obtained its structure factor,  $S(Q)$ . The available  $Q$  range was up to  $\sim 22 \text{ \AA}^{-1}$ , owing to the fact that data collection were conducted up to  $37^\circ$  of  $2\theta$ . The resultant  $S(Q)$  is in overall agreement with the results for glass.<sup>20</sup> The pattern of  $S(Q)$  has similar characteristics: an asymmetric principal peak located at  $4.5 \text{ \AA}^{-1}$  (dashed arrow) and a small peak at  $\sim 3 \text{ \AA}^{-1}$ . The first peak in  $S(Q)$ , the so-called first sharp diffraction peak (FSDP: e.g., Ref. 21), appears at  $1.691 \text{ \AA}^{-1}$  (solid arrow). The FSDP is widely understood as the peak reflecting the intermediate range ordering in network forming glasses and liquids (e.g., Ref. 21). The position of the FSDP for liquid NaAlSi<sub>3</sub>O<sub>8</sub> has been reported as  $1.65 \text{ \AA}^{-1}$ ,<sup>22</sup> which is slightly lower in  $Q$  (hence larger atomic distance in real space) than in our result for glass. This can be explained as due to the temperature effects. The intensity of the FSDP in our measurement is slightly weaker than the results obtained by a monochromatic x-ray source reported in a previous study.<sup>20</sup> This may indicate that absorption effects of the material surrounding the sample have not been completely corrected. This problem can affect the intensity of the peak in  $G(r)$ , which provides the coordination numbers of each atomic pair. However, it does not affect the position of the peaks in  $G(r)$ , which represents the interatomic distance for each atomic pairs.

The radial distribution function,  $D(r)$ , obtained in this study was comparable with previous results<sup>20</sup> as shown in Fig. 5. Overall, the positions of the peaks are consistent with each other. The major difference in the configuration of the  $D(r)$  is the distinctness of the peaks, which is due to the difference in the limitation of the  $Q$  range. Previous data were collected up to  $\sim 15 \text{ \AA}^{-1}$ , whereas our measurements were obtained up to  $\sim 22 \text{ \AA}^{-1}$ . This larger  $Q$  range has significantly improved the resolution in the radial distribution function. The T–O bond length ( $r_{T-O}$ ) is  $1.634 \text{ \AA}$  [Fig. 4(b)], which is consistent with that obtained in previous studies. On the other hand, the T–T bond length ( $r_{T-T}$ ) for the present

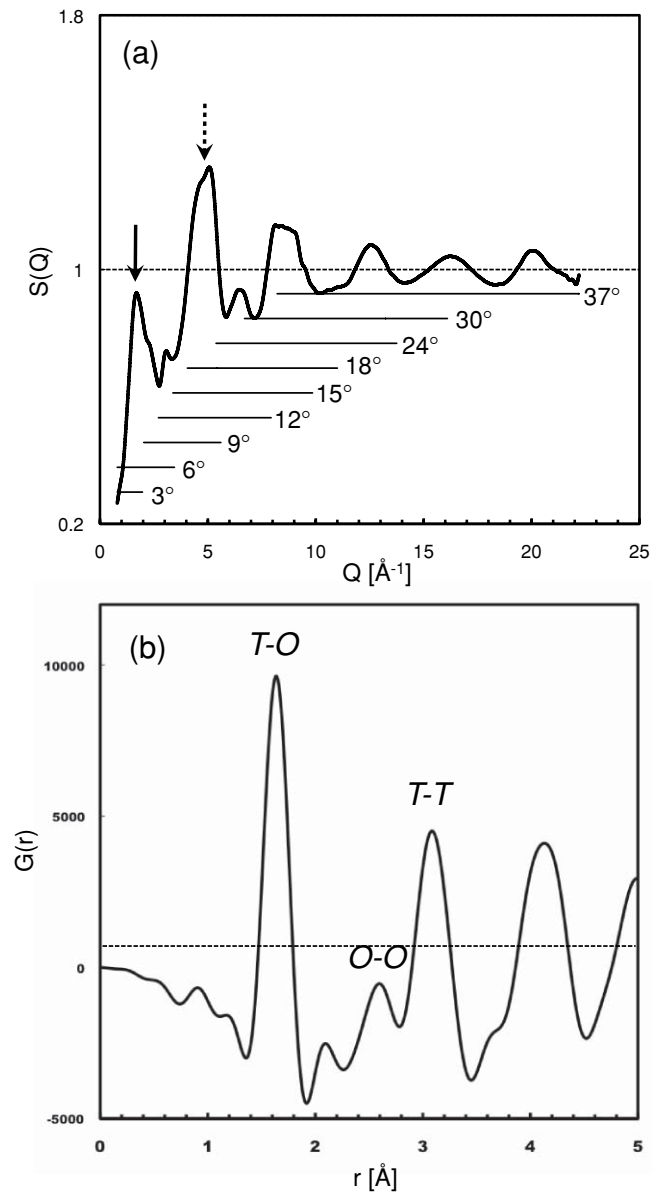


FIG. 4. Structure factor,  $S(Q)$ , (upper) and reduced radial distribution function,  $G(r)$ , (lower) for NaAlSi<sub>3</sub>O<sub>8</sub> glass at 1 atm. Bars in the upper figure indicate the covering  $Q$  range by each diffraction angles.  $T$  in the figure indicates the atoms of Si and Al. Arrows indicate the FSDP (arrow with solid line) and principal peak (arrow with dotted line).

glass is  $3.085 \text{ \AA}$ , slightly shorter than that of the previous study ( $r_{T-O} = 1.63 \text{ \AA}$ ;  $r_{T-T} = 3.12 \text{ \AA}$ : Ref. 20). The peak at  $2.600 \text{ \AA}$  can be assigned as the O–O atomic pair. Although the O–O peak appears in the radial distribution function obtained in previous studies, the position has never been reported. The average T–O–T angle ( $\alpha$ ) is determined to be  $141.5^\circ$ , which can be calculated from the relationship between  $r_{T-O}$  and  $r_{T-T}$  ( $\alpha = 2\arcsin[r_{T-T}/2r_{T-O}]$ ). This angle is smaller than that reported in the previous study ( $\alpha = 146^\circ$ ). The O–T–O bond angle ( $\beta$ ) is calculated to be  $105.4^\circ$ , using  $r_{T-O}$  and  $r_{O-O}$  ( $\beta = 2\arcsin[r_{O-O}/2r_{T-O}]$ ). The  $\alpha$  and  $\beta$  derived in this study are reasonable compared to previous simulation results on liquid NaAlSi<sub>3</sub>O<sub>8</sub>.<sup>23</sup>

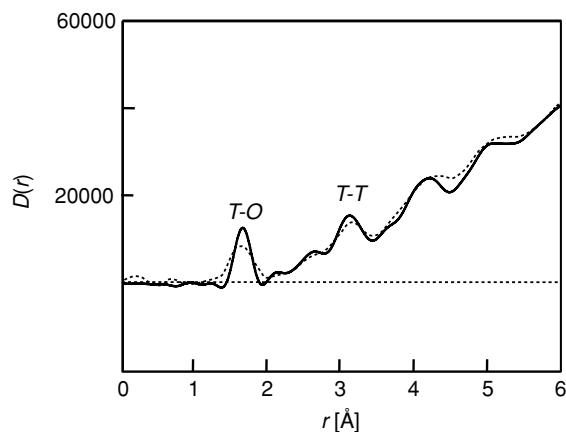


FIG. 5. Radial distribution functions,  $D(r)$ , of  $\text{NaAlSi}_3\text{O}_8$  glass at 1 atm. Solid and dashed line are the present study and previous result taken from Taylor and Brown (1979), respectively.

### B. Application to high-pressure XRD on silicate liquid structure

The relationship between ram load and cell pressure was checked with a cell assembly in which a pressure standard ( $\text{MgO}$ ) was loaded (Fig. 6). Pressure was successfully generated up to  $\sim 8$  GPa without anvil damage. The difference in pressures between two locations, one inside of the sample container ( $a$  in Fig. 6) and one outside ( $b$  in Fig. 6), was closely examined. This difference was generally within 0.8 GPa even at room temperature, indicating that the pressure standard located outside the sample chamber represents a reliable pressure measurement for the sample.

Diffraction patterns of liquid  $\text{NaAlSi}_3\text{O}_8$  collected at 5.3 GPa and 1873 K is shown in Fig. 7. The duration of the

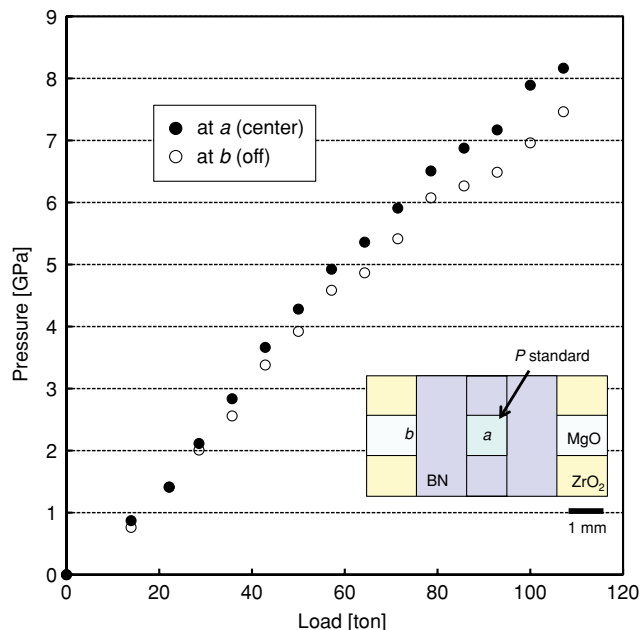


FIG. 6. (Color online) A relationship between load and pressure and the difference in pressure between the center of the assembly and  $\sim 2$  mm off center. Illustration in the figure shows the center of the assembly for the test experiment.  $a$  and  $b$  in the figure indicate schematically the location where the pressure was measured.

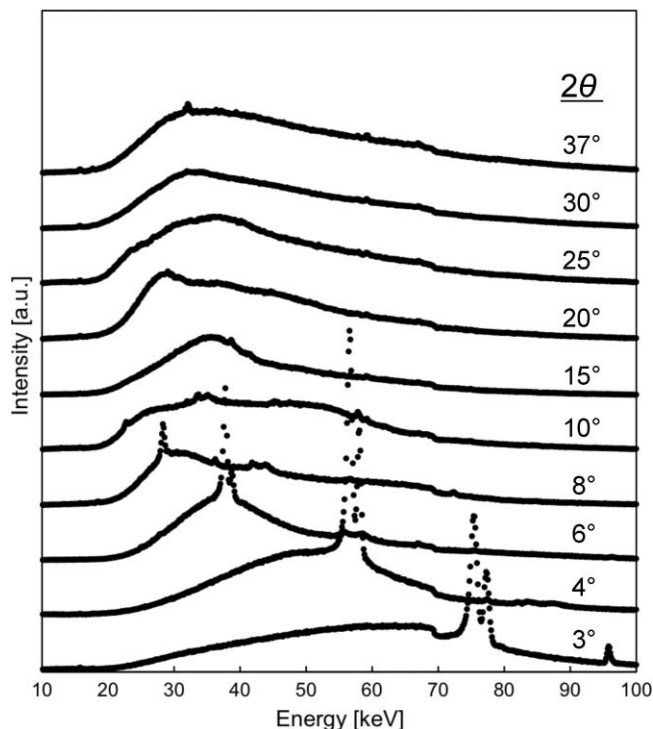


FIG. 7. Diffraction patterns for the liquid  $\text{NaAlSi}_3\text{O}_8$  collected at 5.3 GPa and 1873 K. Sharp diffraction peaks seen in lower diffraction angles are from graphite and/or boron nitride which are used as a sample container and electrical insulator (Fig. 2).

entire data collection was  $\sim 2$  h. Although sharp peaks from the sample container (graphite) appeared in patterns at lower  $2\theta$  angles, the patterns are of sufficient quality for structural analysis. A small absorption edge at  $\sim 69$  keV is seen in all the patterns, and is identified as tungsten, which is most likely due to the upstream slits because it does not show significant angular ( $2\theta$ ) dependence. In other words, the edge is almost equally included in the patterns. Therefore, it does not seriously affect the normalization of the intensity.

The diffraction patterns shown in Fig. 7 were successfully processed to yield structure factor information shown in Fig. 8. The FSDP becomes sharper and shifts toward higher  $Q$  with increasing pressure. The position of the FSDP is  $2.059 \text{ \AA}^{-1}$  at 5.3 GPa, indicating a shrinkage of the intermediate range ordering of the aluminous silicate network by compression. This result suggests that the intermediate range ordering has been reduced by  $\sim 18\%$  compared to the glass at 1 atm.

The  $G(r)$ , which shows local structure in liquid  $\text{NaAlSi}_3\text{O}_8$  at high-pressure (5.3 GPa), was derived as shown in Fig. 9. In spite of the extension of the  $Q$  range, the individual peaks representing Si–O and Al–O distances still cannot be distinguished. This suggests that the  $Q$  range is not sufficient for the required resolution in  $G(r)$ , and that the proportion of the highly coordinated Al is not large. The Al–O bond length for the four-coordinated Al ( $\text{Al}^{\text{IV}}$ ), which dominates at 1 atm, cannot be distinguished from the Si–O pair due to the similar distance as shown in Fig. 4(b). The peaks may become separated at higher pressures because highly coordinated Al (i.e.,  $\text{Al}^{\text{V}}$ ,  $\text{Al}^{\text{VI}}$ ) cations have longer bond lengths (e.g., the

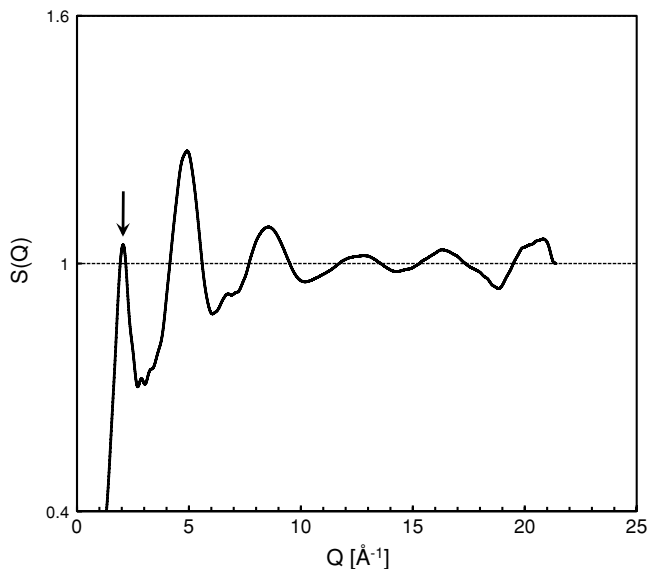


FIG. 8. Structure factor for liquid  $\text{NaAlSi}_3\text{O}_8$  at 5.3 GPa and 1873 K. Arrow indicates the FSDP (see text).

average  $r_{\text{Al-O}}$  of  $\text{Al}^{\text{VI}}$  in jadeite is  $\sim 1.93 \text{ \AA}$  at 1 atm.<sup>24</sup>) Another change in the configuration of the  $G(r)$  can be seen in the peak around  $3 \text{ \AA}$ , which represents the atomic pair of T–T. This initially shows as one broad peak at 1 atm [Fig. 4(b)], but another peak starts to emerge on the long distance side at 5.3 GPa (solid arrow in Fig. 9). The interatomic distance of T–O shows slight shortening ( $1.626 \text{ \AA}$ ). The bond angle of O–T–O ( $\beta$ ) is calculated to be  $\beta = 105.3^\circ$ , based on the T–O and O–O bond lengths ( $r_{\text{O-O}} = 2.585 \text{ \AA}$ ). This result indicates that the local structure of  $\text{SiO}_4$  and  $\text{AlO}_4$  tetrahedra do not show significant changes at least up to 5.3 GPa. On the other hand, the T–O–T bond angle ( $\alpha$ ) changed markedly to  $128.7^\circ$ . This suggests that rearrangement and/or compaction

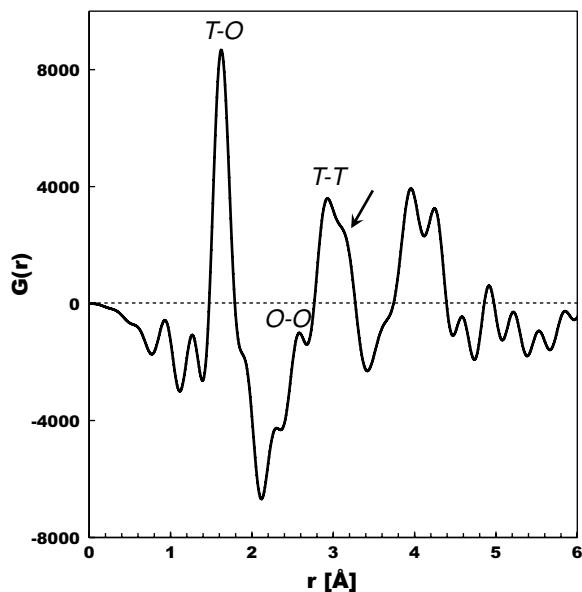


FIG. 9. Reduced radial distribution function for structure factor for liquid  $\text{NaAlSi}_3\text{O}_8$  at 5.3 GPa and 1873 K.  $T$  in figure represents the atoms of Si and Al.

of the aluminous silicate network by compression is the most responsible for densification at least up to the present pressure, as indicated in the change in position of the FSDP.

#### IV. FUTURE WORK

We have demonstrated a successful data collection for a liquid silicate structure at high-pressure with a Paris–Edinburgh press. The present technique can be applied to several experimental methods as follows. (1) Angle dispersive powder diffraction with polychromatic x-ray source [CAESER (Ref. 25)]: the accurate and wide angular accessibility of the present device enables us to achieve more precise structure refinement for a crystalline phase at high-pressure and temperature. (2) High-pressure x-ray microtomography.<sup>26</sup> Similarly, the excellent angular access of the device is helpful for the 3D image reconstruction to observe a sample texture under pressure and/or to investigate the volumetric properties of amorphous and liquid phases with pressure.<sup>27</sup> So far, this method has not been applied to silicate liquid. The present device does not have complete  $360^\circ$  accessibility due to the interference of the press flame. However, we can technically reconstruct a 3D image through such a shadowed region using the data set of 2D image results of pseudo images in the slice images (cf., Ref. 28). (3) Densimetry with x-ray absorption.<sup>29</sup> In order to obtain information on density, we need to determine the initial intensity of the x-rays, the intensity of the x-rays passing through the sample (absorption), and the x-ray transmitting length through the sample in the experiment.<sup>30</sup> The information of the x-ray transmitting length is difficult to measure directly and precisely due to geometrical constraints of the high-pressure apparatus. In our case, we can measure the length directly with the x-ray image using the Paris–Edinburgh type device because the sample can be accessed from  $90^\circ$  by rotating the device.

Further applications can be done for elastic wave velocity measurement with ultrasonic interferometry, as well as other x-ray scattering techniques. Thus, the new setup may provide a platform for comprehensive physical property measurements on silicate liquids, for a better understanding of the physics of these materials.

#### ACKNOWLEDGMENTS

We thank the journal editors and anonymous reviewer for their kind handling and constructive comments. The present experiments were performed at HPCAT (Sector 16), Advanced Photon Source (APS), Argonne National Laboratory. HPCAT is supported by CIW, CDAC, UNLV, and LLNL through funding from DOE-NNSA, DOE-BES, and NSF. APS is supported by DOE-BES, under Contract No. DE-AC02-06CH11357. The PEP system was developed at GeoSoilEnviroCARS (Sector 13), APS. GeoSoilEnviroCARS is supported by the National Science Foundation–Earth Sciences (EAR-0622171) and Department of Energy–Geosciences (DE-FG02-94ER14466). Use of the Advanced Photon Source was supported by the U.S. Department of Energy, Office of Science, Office of Basic Energy Sciences, under Contract No. DE-AC02-06CH11357.

Y. W. acknowledges NSF Grant No. EAR 0711057 for the development of this facility. This study was also supported by global COE program “Deep Earth Mineralogy” and Grant-in-Aid for Scientific Research (A) to T.I. We thank Ellen La Rue (GSECARS) and Curtis Kenny-Benson (HPCAT) for their excellent technical support during the development.

- <sup>1</sup>A. Yamada, T. Inoue, S. Urakawa, K. Funakoshi, N. Funamori, T. Kikegawa, H. Ohfuji, and T. Irifune, *Geophys. Res. Lett.* **34**, L10303 (2007).
- <sup>2</sup>A. Yamada, T. Irifune, H. Sumiya, Y. Higo, T. Inoue, and K. Funakoshi, *High Press. Res.* **28**, 255 (2008).
- <sup>3</sup>N. Funamori, S. Yamamoto, T. Yagi, and T. Kikegawa, *J. Geophys. Res.* **109**, B03203 (2004).
- <sup>4</sup>S. Klotz, G. Hamel, and J. Frelat, *High Press. Res.*, **24**, 219 (2004).
- <sup>5</sup>G. Monaco, S. Falconi, W. A. Crichton, and M. Mezouar, *Phys. Rev. Lett.* **90**, 255701 (2003).
- <sup>6</sup>G. Morard, M. Mezouar, N. Rey, R. Poloni, A. Merlen, S. L. Floch, P. Toulemonde, S. Pascarelli, A. San-Miguel, C. Sanloup, and G. Fiquet, *High Press. Res.* **27**, 223 (2007).
- <sup>7</sup>S. Speziale, C.-S. Zha, S. D. Duffy, R. J. Hemley, and H.-K. Mao, *J. Geophys. Res.* **106**, 515 (2001).
- <sup>8</sup>F. R. Boyd and J. L. England, *J. Geophys. Res.* **68**, 311 (1963).
- <sup>9</sup>N. Nishikawa and T. Iijima, *Bull. Chem. Soc. Jpn.* **57**, 1750 (1984).
- <sup>10</sup>K. Funakoshi, Ph.D. thesis, Tokyo Institute of Technology, 1997.
- <sup>11</sup>K. Tamura and S. Hoshokawa, *Phys. Rev. B.*, **58**, 9030 (1998).
- <sup>12</sup>Y. Katayama, *J. Non-Cryst. Solids*, **312–314**, 8 (2002).
- <sup>13</sup>K. Fuchizaki, T. Hase, A. Yamada, N. Hamaya, Y. Katayama, and K. Funakoshi, *J. Chem. Phys.* **130**, 121101 (2009).
- <sup>14</sup>J. A. Ibers and W. C. Hamilton, *International Tables for X-Ray Crystallography* (Kynoch, Birmingham, 1974).
- <sup>15</sup>D. T. Cromer and J. B. Mann, *J. Chem. Phys.* **47**, 1892 (1967).
- <sup>16</sup>D. T. J. Cromer, *J. Chem. Phys.*, **50**, 4867 (1969).
- <sup>17</sup>F. Hadju, *Acta. Cryst.* **A29**, 10 (1971).
- <sup>18</sup>R. Kaplow, S. L. Strong, and B. L. Averbach, *Phys. Rev.* **138**, A1336 (1965).
- <sup>19</sup>J. D. Bass, *Mineral Physics and Crystallography: A Hand Book of Physical Constants* (AGU Reference Shelf 2 1995), p. 45.
- <sup>20</sup>M. Taylor and G. E. Brown, *Geochim. Cosmochim. Acta*, **43**, 61 (1979).
- <sup>21</sup>S. R. Elliott, *Phys. Rev. Lett.* **67**, 711 (1991).
- <sup>22</sup>M. Okuno and F. Marumo, *Mineral. J.* **11**, 180 (1982).
- <sup>23</sup>A. Suzuki, E. Ohtani, K. Funakoshi, H. Terasaki, and T. Kubo, *Phys. Chem. Miner.* **29**, 159 (2002).
- <sup>24</sup>M. Cameron, S. Sueno, and C. T. Prewitt, *Am. Mineral.* **58**, 594 (1973).
- <sup>25</sup>Y. Wang, T. Uchida, R. V. Dreele, M. L. Rires, N. Nishiyama, K. Funakoshi, A. Nozawa, and H. Kaneko, *J. Appl. Cryst.* **37**, 947 (2004).
- <sup>26</sup>Y. Wang, T. Uchida, F. Westferro, M. L. Rivers, N. Nishiyama, J. Gebhardt, C. E. Leshner, and S. R. Sutton, *Rev. Sci. Instrum.* **76**, 073709 (2005).
- <sup>27</sup>C. E. Leshner, Y. Wang, S. Gaudio, A. Clark, N. Nishiyama, and M. Rivers, *Phys. Earth Planet. Inter.* **174**, 292 (2009).
- <sup>28</sup>S. Urakawa, H. P. Terasaki, K. Funakoshi, K. Uesugi, and S. Yamamoto, *J. Phys.: Conf. Ser.* **215**, 012026 (2010).
- <sup>29</sup>Y. Katayama, K. Tsuji, H. Kanda, H. Nosaka, K. Yaoita, T. Kikegawa, and O. Shimomura, *J. Non-Cryst. Solids* **205–207**, 451 (1996).
- <sup>30</sup>T. Sakamaki, E. Ohtani, S. Urakawa, A. Suzuki, and Y. Katayama, *Am. Mineral.* **95**, 144 (2010).